

# IC 2560 and UGC 3193 megamaser AGN black hole mass estimations using general relativity

Adriana González-Juárez and Alfredo Herrera-Aguilar

Instituto de Física Luis Rivera Terrazas (IFUAP), Benemérita Universidad Autónoma de Puebla, Puebla 72570, México

Received Month XX, XXXX; accepted Month XX, XXXX

## ABSTRACT

*Context.* An important current problem regarding the characterization of the central engine of active galactic nuclei (AGNs) consists in determining the parameters of the black holes (BHs) hosted at their cores, especially their mass.

*Aims.* Therefore, we aim to apply a full general relativistic method to estimate the parameters of the central supermassive BHs hosted at the center of the IC 2560 and UGC 3193 galaxies.

*Methods.* In order to achieve this aim we implement a general relativistic BH rotation curves' method and estimate the BH parameters by fitting megamaser astrophysical data available in the literature with the help of a Bayesian statistical method.

*Results.* We calculate the mass of the aforementioned BHs, their positions on the sky as well as the recession velocities of the host galaxies. On the basis of our estimations, we compute for the first time the BH mass of the UGC 3193 AGN. We also calculate the gravitational redshift of the closest maser to these BHs, a general relativistic effect produced by the curvature of spacetime that has no Newtonian analogue.

**Key words.** black hole physics – masers – galaxies: nuclei – galaxies: high-redshift – methods: statistical.

## 1. Introduction

An interesting process in galactic dynamics regards the mechanisms that lead to the creation of supermassive black holes (BHs) in the center of most galaxies (see, e.g., Kormendy & Richstone 1995). The current understanding that supermassive BHs are found at the core of many galaxies arose with the discovery of quasars and AGNs, where huge rates of luminous radiation are produced within small compact volumes (Celotti et al. 1999). Besides, the presence of a supermassive BH at the core of these AGNs plausibly explains the spectral information coming from gas particles that revolve around it and attain velocities of thousands of kilometers per second. A relevant issue regarding the characterization of AGNs consists in determining the mass, the spin, the distance as well as other parameters of the BHs hosted at their cores. In particular, determining the BH masses in AGNs is essential for understanding the fundamental properties of their central engines, as well as for gaining insights into their growth and coevolution with their host galaxy (see, e.g., Kormendy & Ho 2013, Greene et al. 2016).

Water megamaser systems consist of  $\text{H}_2\text{O}$  vapor clouds that emit intense stimulated microwave radiation at 22 GHz and offer a powerful tool for investigating the very core of AGNs and their surrounding environments. These astrophysical systems are very luminous water masers, typically  $\sim 10^6$  times more luminous than Galactic maser sources, hosted on accretion disks at circumnuclear regions of several AGNs. Their extremely high surface brightness enables a detailed mapping at sub-milliarcsecond resolution using Very Long Baseline Interferometry (VLBI), allowing for a direct way to study AGN structures and dynamics at sub-parsec scales.

On the other hand, the maser disks themselves provide valuable insights into the dynamics around supermassive BHs. In

particular, the maser disk size correlates with the central BH mass: The mean radius of maser disks increases with BH mass (see Wardle & Yuset-Zadech 2012, Gao et al. 2016b, Kuo et al. 2024). Besides, according to a recent model developed by Kuo et al. (2024), maser disks also exhibit interesting behavior related to their size, which is influenced by physical processes and the interplay of various factors. Namely, the outer radius of the disk is mainly defined by the maximum X-ray heating rate coming from the central engine or by the minimum gas density required for efficient maser emission, depending on a combination of the Eddington ratio, the BH mass, and the disk mass. Meanwhile, the disk inner radius for maser action is determined by the dust sublimation radius.

Within this context, the Megamaser Cosmology Project<sup>1</sup> (MCP) has studied over 20 megamaser disks in AGNs (see, for instance, Reid et al. 2009, Kuo et al. 2011, Kuo et al. 2013, Gao et al. 2016a, Gao et al. 2016b, Zhao et al. 2018, Pesce et al. 2020a, Kuo et al. 2020, and Pesce et al. 2020b) making use of VLBI techniques with the Very Large Baseline Array (VLBA), the Radio Telescope Effelsberg (ET), the Robert C. Byrd Green Bank Telescope (GBT) and the Karl G. Jansky Very Large Array (VLA). This project has managed to determine the Hubble constant value  $H_0$  with 4% uncertainty (Pesce et al. 2020b), and to estimate the mass of the BH hosted at the center of those galaxies to percent-level accuracy (Kuo et al. 2011, Gao et al. 2016b) as

<sup>1</sup> The MCP is a key project of the National Radio Astronomy Observatory (NRAO), in collaboration with the Cosmic Microwave Background project from Wilkinson Microwave Anisotropy Probe and Planck missions, that seeks to determine the Hubble constant value by making use of megamaser observations of galaxies moving within the Hubble flow, Reid et al. (2009). <https://safe.nrao.edu/wiki/bin/view/Main/MegamaserCosmologyProject>

well as the distance to them, disregarding the use of distance ladders, gravitational lenses or standard candles (Reid et al. 2009, Gao et al. 2016a, Pesce et al. 2020a).

Within this framework, in order to determine the parameters of the supermassive BHs located at the core of AGNs, a full general relativistic method was developed in Herrera-Aguilar & Nucamendi (2015) and Banerjee et al. (2022) for spinning BH configurations, allowing for the potential detection of relativistic effects within such astrophysical systems. A static version of this method was applied to estimate the mass-to-distance ratio<sup>2</sup> of the central BHs living in several AGNs: The case of NGC 4258 was addressed in Nucamendi et al. (2021), whereas TXS-2226-184 was studied in Villalobos-Ramírez et al. (2022); fourteen more galaxies previously considered by the MCP were approached in Villaraos et al. (2022) and González-Juárez et al. (2024). In these works, the authors also quantified general and special relativistic effects, namely, the gravitational redshift (generated by the curvature of spacetime in the BH vicinity) experienced by the closest maser to the BH, and the peculiar velocity of the host galaxy with respect to the Earth, accounted for by a special relativistic boost.

In this paper we implement the general relativistic method and a Bayesian statistical fit to estimate the BH parameters of two more megamaser systems that were not considered by the MCP. For the BH anchored at the heart of IC 2560 we constrain four parameters, namely, the  $M/D$  ratio, the  $x$ - and  $y$ - offsets of the BH position on the sky, and its recession velocity  $v_{rec}$ ; we further estimate three parameters for the BH hosted at the nucleus of UGC 3193: the  $M/D$  ratio, the  $x$ -offset of the BH position, and the  $v_{rec}$ . The statistical fit did not render a most probable value for the  $y$ -offset of the BH position, probably because of the strong warping that the maser disk displays.

This paper is organized as follows: In section 2 we present the BH rotation curve general relativistic model, whereas in Sec. 3 we briefly review the Bayesian statistical method that we apply to it and present the results of the fit. Finally, we conclude with a comparison of our findings with previous results and a brief discussion in Sec. 4.

## 2. Frequency shift in general relativity

In this Section we review the general relativistic model that we employ to describe BH rotation curves. This model is based on a metric approach developed in (Herrera-Aguilar & Nucamendi 2015) and (Banerjee et al. 2022) that makes use of observational quantities, namely, the redshift and blueshift of photons emitted by massive particles orbiting the BH and their orbital parameters.

This method was also implemented in Nucamendi et al. (2021) using a Schwarzschild metric in order to fit the parameters of the BH hosted at the core of the NGC 4258 AGN. In this work, water megamaser clouds that lie on the accretion disk and circularly revolve around the central BH of the AGN were considered as test particles that are stimulated by the BH, making them to emit photons in a very coherent way. Both the maser clouds geodesically orbiting the BH and the photons they emit feel the gravitational field of the BH and keep memory of its properties. Thus, when we measure on Earth the shift in the photon's frequency at certain orbital positions of the masers, we obtain information about the BH parameters as well.

We further derive the general relativistic formulas for the total frequency shift experienced by photons emitted by massive

<sup>2</sup> This ratio refers to the BH mass  $M$  divided by its distance to the observer  $D$ .

bodies orbiting a receding or approaching Schwarzschild BH with respect to a distant observer with constant peculiar velocity  $v_p$ . We also expand these expressions in terms of the  $m/r_e$  and  $v_p/c$  ratios in order to see what is the magnitude of the general and special relativistic corrections to the corresponding Newtonian formula. We finally compose the frequency shifts generated by the special relativistic boost and the expansion of the Universe in order to account for the recessional redshift of BHs hosted at the core of galaxies within the Hubble flow.

### 2.1. Geodesic motion of massive particles around the Schwarzschild BH

We start by recalling the expression for the Schwarzschild metric

$$ds^2 = \frac{dr^2}{f} + r^2(d\theta^2 + \sin^2\theta d\varphi^2) - f dt^2, \quad f = 1 - \frac{2m}{r}, \quad (1)$$

where  $m$  is the total mass of the BH in natural units ( $G = 1 = c$ ). The motion of massive and massless particles takes place in the gravitational field of this line element.

The per mass unit conserved energy  $E$  and axial angular momentum  $L$  of a massive particle in geodesic motion in the Schwarzschild background due to the existence of the temporal  $\xi^\mu = \delta_t^\mu$  and rotational  $\psi^\mu = \delta_\varphi^\mu$  Killing vector fields read

$$E = -g_{\mu\nu}\xi^\mu U^\nu = -g_{tt}U^t, \quad L = g_{\mu\nu}\psi^\mu U^\nu = g_{\varphi\varphi}U^\varphi. \quad (2)$$

where  $g_{\mu\nu}$  is the metric tensor and  $U^\mu$  is the particle four-velocity.

These relations allow us to express the four-velocity components  $U^t$  and  $U^\varphi$  as follows

$$U^t = -\frac{E}{g_{tt}}, \quad U^\varphi = \frac{L}{g_{\varphi\varphi}}. \quad (3)$$

The momentum conservation in GR restricts the four-velocity to  $U^2 = -1$ , giving

$$g_{rr}(U^r)^2 + g_{\theta\theta}(U^\theta)^2 + \frac{E^2}{g_{tt}} + \frac{L^2}{g_{\varphi\varphi}} + 1 = 0, \quad (4)$$

Since the Schwarzschild metric possesses spherical symmetry, we can always restrict particle motion to the equatorial plane  $\theta = \pi/2$  ( $U^\theta = 0$ ), obtaining the following non-relativistic energy conservation equation

$$\frac{1}{2}(U^r)^2 + \frac{1}{2}\left(1 - \frac{2m}{r}\right)\left(\frac{L^2}{r^2} + 1\right) = \frac{E^2}{2}, \quad (5)$$

which defines an effective potential of the form

$$V_{eff} = \frac{1}{2}\left(1 - \frac{2m}{r}\right)\left(\frac{L^2}{r^2} + 1\right). \quad (6)$$

By further considering circular motion ( $U^r = 0$ ), we require to have a minimum in the effective potential, obtaining the following conditions

$$V_{eff} = \frac{E^2}{2}, \quad \partial_r V_{eff} = 0. \quad (7)$$

From these relations we obtain  $E$  and  $L$  as follows:

$$E = \frac{1 - \frac{2m}{r}}{\sqrt{1 - \frac{3m}{r}}}, \quad L = \pm r \sqrt{\frac{m}{r} \left(1 - \frac{3m}{r}\right)}. \quad (8)$$

where the  $\pm$  signs correspond to clockwise and counterclockwise motion of the test particles with respect to a distant observer. These relations are very interesting since they point out that both energy and angular momentum of massive particles in circular geodesic motion are divided by the factor  $\sqrt{1 - 3m/r}$ .

Therefore, the non-trivial components of the four-velocity read

$$U^t = \frac{1}{\sqrt{1 - \frac{3m}{r}}}, \quad U^\varphi = \pm \frac{1}{r} \sqrt{\frac{m}{1 - \frac{3m}{r}}}. \quad (9)$$

It is also crucial to note that the energy of a massive particle in circular geodesic motion differs from that of a *static* particle in the background of a Schwarzschild BH (see Schutz 2009). Moreover, a static particle cannot be in geodesic motion in the sense that it would necessarily move towards the BH. Therefore, in order to model general relativistic effects such as the gravitational frequency shift or the time dilation of particle's motion on accretion discs in a correct way, one has to consider massive particles circularly orbiting the central BH.

## 2.2. Geodesic motion of photons in the Schwarzschild metric

We now turn to describe the motion of photons emitted by massive particles in the Schwarzschild BH metric. The propagation of photons is parameterized by their four-momentum  $k^\mu$ . By following the same line of reasoning used for massive particles, we shall have two conserved quantities, energy and axial angular momentum, along the photons path due to the existence of the temporal and rotational Killing vector fields:

$$E_\gamma = -g_{tt}k^t, \quad L_\gamma = g_{\varphi\varphi}k^\varphi. \quad (10)$$

These relations allow us to express the  $k^t$  and  $k^\varphi$  components as

$$k^t = -\frac{E_\gamma}{g_{tt}} = \frac{E_\gamma}{1 - \frac{2m}{r}}, \quad k^\varphi = \frac{L_\gamma}{g_{\varphi\varphi}} = \frac{L_\gamma}{r^2}. \quad (11)$$

Moreover, the photon paths are restricted to the condition  $k^2 = 0$ , which on the equatorial plane yields an expression for  $k^r$ :

$$k^r = \sqrt{E_\gamma^2 - \left(1 - \frac{2m}{r}\right) \frac{L_\gamma^2}{r^2}}, \quad (12)$$

completely determining all the nontrivial components of the photon's four-momentum since the  $k^\theta = 0$  due to the motion on the equatorial plane.

## 2.3. The frequency shift in Schwarzschild background

We further define the photon frequency as a general relativistic invariant  $\omega = -k_\mu U^\mu$ . This quantity can be measured at the points of emission and detection, allowing us to arrive at the following expression for the Schwarzschild frequency shift of these photons in the equatorial plane

$$1 + z_{Schw_{1,2}} = \frac{\omega_e}{\omega_d} = \frac{(E_\gamma U^t - L_\gamma U^\varphi - g_{rr}k^r U^r)_e}{(E_\gamma U^t - L_\gamma U^\varphi - g_{rr}k^r U^r)_d} = \frac{(U^t - b_\mp U^\varphi)_e}{(U^t - b_\mp U^\varphi)_d}, \quad (13)$$

where the indices  $_{1,2}$  refer to redshift and blueshift, respectively, while the subindices  $_e$  and  $_d$  denote an emission and detection

points. Here we have considered that the emitter and the detector are in geodesic circular motion around the BH, and we have defined the light bending parameter (also called apparent impact parameter) at the points at which the velocity gain paths of the test particles are the longest (around the disk midline) in order to maximize the possibilities of frequency shift detection:

$$b_\pm \equiv \frac{L_\gamma}{E_\gamma} = \pm \sqrt{-\frac{g_{\varphi\varphi}}{g_{tt}}} = \pm \frac{r}{\sqrt{1 - \frac{2m}{r}}}, \quad (14)$$

where now the  $\pm$  signs correspond to the massive particle's motion either side of the observer's line of sight. This quantity measures in fact the deflection of light generated by the gravitational field of the BH, it is conserved from the moment of emission till detection ( $b_e = b_d$ ), and depends purely on the metric.

By considering a static observer located far away from the BH, i.e. when  $r_d \rightarrow \infty$ , its four-velocity simplifies to  $U^\mu|_d = (1, 0, 0, 0)$ , rendering the following total frequency shift

$$1 + z_{Schw_{1,2}} = \frac{1}{\sqrt{1 - \frac{3m}{r_e}}} \left( 1 \pm \sqrt{\frac{m}{1 - \frac{2m}{r_e}}} \right), \quad (15)$$

where the  $\pm$  signs correspond to the  $_{1,2}$  indices and refer to the redshift and the blueshift, respectively, and  $r_e$  is the orbital radius of the emitter (the megamaser features). Here it is suitable to use the approximation  $\Theta \approx r_e/D$ , where  $\Theta$  is the angular distance between a given maser and the BH in our model and estimations.

From this expression, it is quite natural to define the gravitational redshift in terms of the temporal component of the contraction that defines the Schwarzschild frequency shift (13), a quantity that encodes the curvature of spacetime generated by the BH mass and has no Newtonian analogue:

$$1 + z_g = \frac{1}{\sqrt{1 - \frac{3m}{r_e}}}, \quad (16)$$

whereas the kinematic redshift and blueshift either side of the BH are determined by the second term:

$$z_{kin_\pm} = \pm \sqrt{\frac{\frac{m}{r_e}}{\left(1 - \frac{3m}{r_e}\right)\left(1 - \frac{2m}{r_e}\right)}} \quad (17)$$

that also modifies the Newtonian kinematic frequency shift.

We remark that in this work we only use the redshift and blueshift of masers located at the points where their velocity gain paths are the longest, i.e., in the vicinity of the midline of the disk. The use of systemic maser features still remains pending.

In the weak field limit, by expanding  $z_{Schw_{1,2}}$  with respect to  $m/r_e$  we see that the leading term is given by the redshift and blueshift of photons corresponding to rotational motion in the Newtonian picture, whereas the next-to-leading term renders a general relativistic correction due to the gravitational redshift

$$z_{Schw_{1,2}} \approx z_{kin_\pm} + z_g + \dots = \pm \sqrt{\frac{m}{r_e}} + \frac{3}{2} \frac{m}{r_e} + \dots; \quad (18)$$

here the first term constitutes the first order approximation of the kinematic frequency shift (17), while the second item represents the first order approximation of the gravitational redshift (16).

#### 2.4. A receding or approaching BH and the total redshift

Now we consider that the Schwarzschild BH is locally receding from or approaching to the distant observer as a whole entity with a constant peculiar velocity  $v_p$ . This local motion can be described by a special relativistic boost since it is not generated by the Universe's expansion and produces, in turn, a special relativistic redshift or blueshift that we call  $z_{boost}$  with the following definition (see Rindler 1982):

$$1 + z_{boost} = \gamma(1 + \beta \cos \kappa), \quad \gamma = 1/\sqrt{1 - \beta^2}, \quad \beta = v_p/c, \quad (19)$$

where  $\kappa$  is the angle between the direction of the peculiar velocity and the LOS (we shall consider  $\kappa = 0$  henceforth for simplicity),  $v_p \equiv z_p c$ , and we have called  $z_p$  the redshift or blueshift expressed in terms of the peculiar velocity  $v_p$  of the galaxy hosting the BH. This quantity is independent of the BH mass and has a different nature compared to the Schwarzschild redshift since it is generated by a special relativistic effect, i. e. by a change of reference frame moving with velocity  $v_p$  with respect to the reference frame of a distant observer in flat spacetime.

By further composing the Schwarzschild and the special relativistic frequency shifts according to Davis & Scrimgeour (2014) we obtain the local redshift:

$$1 + z_{loc1,2} = (1 + z_{Schw1,2})(1 + z_{boost}). \quad (20)$$

The local redshift (or blueshift),  $z_{loc1,2}$ , is the quantity that one measures from a photon's source revolving a receding or approaching BH along with its position in the sky.

By performing a double expansion of the local frequency shift in terms of the  $m/r_e$  ratio and the special relativistic boost parameter  $v_p/c$ , we obtain up to 1.5 order (see Nucamendi et al. 2021)

$$\begin{aligned} z_{tot1,2} &\approx z_{kin\pm} + z_p + z_g + z_p z_{kin\pm} + z_{kin\pm} z_g + \dots \\ &= \pm \sqrt{\frac{m}{r_e}} + \frac{v_p}{c} + \frac{3m}{2r_e} \pm \frac{v_p}{c} \sqrt{\frac{m}{r_e}} \pm \frac{5}{2} \left(\frac{m}{r_e}\right)^{\frac{3}{2}} + \dots, \end{aligned} \quad (21)$$

where additionally to the items obtained in the expansion (18), now the second term corresponds to the receding or approaching peculiar velocity of the BH with respect to a distant observer; the fourth term constitutes a combined effect of kinematic and boost redshifts, called kinematic boosted redshift, and the fifth term denotes a composed effect of the gravitational redshift with the kinematic frequency shift; finally, ellipses stand for higher order contributions that become important when the orbiting objects are very close to the BHs.

#### 2.5. The cosmological redshift due to Universe's expansion

In order to have a more realistic modelling of the recessional redshift,  $z_{rec}$ , of BHs hosted at galactic cores that are within the Hubble flow we also need to take into account the cosmological redshift,  $z_{cosm}$ , i.e. the stretching of photons' wavelength produced by the expansion of the Universe.

Thus, the recessional redshift accounting for both local and cosmological motion of galaxies within the Hubble flow reads

$$1 + z_{rec} = (1 + z_{boost})(1 + z_{cosm}), \quad (22)$$

where the cosmological redshift depends on the metric chosen to describe the expansion of the Universe.

However, the Schwarzschild metric we use in our model is static and does not provide information about the Universe's expansion. On the other hand, the special relativistic frequency

shift (19) does not depend on the metric either, leading to a degeneracy of the cosmological and the peculiar redshifts when performing statistical estimations of BH parameters using astrophysical observational data (since none of them depend on the metric). Therefore, in order to avoid this degeneracy, in this work we will fit the total recessional redshift (22) instead of its separate components.

Thus, the expression for the total redshift of photons composing the Schwarzschild frequency shift and the recessional redshift as a first approximation reads

$$1 + z_{tot1,2} = (1 + z_{Schw1,2})(1 + z_{rec}). \quad (23)$$

This is the formula that we shall use in order to determine the BH parameters using Bayesian statistical fits of observational data.

### 3. Bayesian statistical model

In order to further implement the general relativistic method to fit real megamaser astrophysical data, we need to develop a Bayesian statistical model that takes into account the positions and velocities of redshifted and blueshifted water masers (located close to the midline) along with their corresponding uncertainties. This statistical method is based on a Monte Carlo method that makes use of Markov chains and consists of a least squares  $\chi^2$  fit of the following parameters: the BH mass-to-distance ratio,  $M/D$ , its recessional velocity,  $z_{rec}$ , and its position on the sky (either along just the  $x$ -offset or both the  $x$ - and  $y$ -offsets). In a real maser map, the detected spots do not lie perfectly on the midline and are spread around it. Therefore, following an original idea of Herrnstein et al. (2005), we introduce into our model a small dispersion in the azimuthal angle  $\varphi - \varphi_0$  that encodes the departure of the redshifted and blueshifted masers from a fixed value  $\varphi_0$  (we set  $\varphi_0 = 0$  corresponding to the midline). We fix the amplitude in the scattering angle by choosing the smallest value that renders a reduced  $\chi^2$  close to unity. Thus, the Bayesian statistical model is given by

$$\chi^2 = \sum_{k=1} \frac{[z_{k,obs} - (1 + z_{grav} + \sin \theta_0 \cos \varphi z_{kin\pm})(1 + z_{rec}) + 1]^2}{\sigma_{z_{tot1,2}}^2 + \sin^2 \theta_0 z_{kin\pm}^2 (1 + z_{rec})^2 \sin^2 \varphi \delta\varphi^2} \quad (24)$$

where  $\sigma_{z_{tot1,2}} = |\delta z_{tot1,2}|$  is the uncertainty of the total redshift,  $\theta_0$  stands for the inclination angle,  $\delta\varphi$  stands for the induced uncertainties of the maser spread and we have assumed small variations  $\delta\varphi \ll 1$ . The error of the total redshift  $\sigma_{z_{tot1,2}}^2$  has the following form:

$$\delta z_{tot1,2} = (\delta z_{grav} + \delta z_{kin\pm})(1 + z_{rec}), \quad (25)$$

where

$$\delta z_{grav} = (1 + z_{grav})^3 \left(\frac{-3m}{2r_e}\right) \frac{\delta r_e}{r_e}, \quad \delta r_e \approx D \delta\Theta, \quad (26)$$

$$\delta z_{kin\pm} = \sin \theta_0 \cos \varphi (z_{kin\pm})^3 \left(\frac{6m^2 - r_e^2}{2mr_e}\right) \frac{\delta r_e}{r_e}, \quad (27)$$

$$\delta\Theta = \sqrt{\left(\frac{x_i - x_0}{\Theta}\right)^2 \delta_x^2 + \left(\frac{y_i - y_0}{\Theta}\right)^2 \delta_y^2}, \quad (28)$$

$$\Theta = \sqrt{(x_i - x_0)^2 + (y_i - y_0)^2}, \quad (29)$$

with  $(x_i, y_i)$  denoting the position of the  $i$ -th megamaser on the sky,  $\{\delta_x, \delta_y\}$  being their corresponding errors, and  $(x_0, y_0)$  standing for the BH position.

### 3.1. Parameter fitting for our galaxies

In order to apply our general relativistic method to the aforementioned galaxies, we make use of the positions and velocities of the megamaser data reported by Kaliszewski & Braatz (2021) and observed by Jan Wagner. Their maser maps are atypical in the sense that they do not display a set of three maser groups symmetrically distributed on the sky<sup>3</sup>. Instead, they show a less symmetrical and less separated disposition of four or more maser groups on the sky (see Fig. 1). By performing a careful analysis of these observational datasets we realize that by building a three-dimensional velocity-position distribution plot, the relevant maser groups are naturally separated into highly redshifted, blueshifted and systemic sets as it can be appreciated in Fig. 2a) for IC 2560 and Fig. 2b) for UGC 3193, respectively. These arrangements take place despite the unclear separation that the megamaser group maps present. Thus, for IC 2560, Fig. 2a) reveals a system of three groups with highly redshifted and blueshifted masers clearly distinguished from a group of systemic masers, rendering a typical maser configuration. In contrast, for UGC 3193, Fig. 2b) yields two groups of highly redshifted and blueshifted photon sources with a total lack of observed systemic masers in agreement with the map considered by Kaliszewski & Braatz (2021).

We further make use of the database reported by these authors and rotate the maser distribution to the equatorial plane according to the prescription of the general relativistic model. We performed this rotation with respect to a given reference position on the sky for each one of the megamaser features: For IC 2560 we chose the origin of the reference system on the sky by considering the centroid of the systemic masers, whereas for UGC 3193 we allocate the reference position at the middle point between the geometrical centers of the redshifted and blueshifted maser spots since systemic masers were not detected at all in this galaxy. The BH offsets for both galaxies were computed with respect to these positions.

We now review the generalities of the work previously done for the selected galaxies, which are summarized in Table 1, and then present our analysis and estimations.

### 3.2. IC 2560

The 22 GHz maser emission in the AGN type 2 Seyfert galaxy IC 2560 was first detected by Braatz et al. (1994). Further VLBI observations performed by Nakai et al. (1998) and Ishihara et al. (2001) confirmed that this maser system possesses a disk structure. The VLBI map for this galaxy is plotted in Fig. 1 according to the observational data reported in Kaliszewski & Braatz (2021) and presents at least 4 groups of maser features within a disk of subparsec diameter, typical for maser disks viewed edge-on from Earth (see, e.g., Braatz & Gugliucci 2008; Braatz et al. 2010).<sup>4</sup> The distance to this galaxy  $D = 39.6 \pm 1.6$  Mpc was calculated with the aid of the 21 cm line velocity of  $2923 \pm 10$  km s<sup>-1</sup> and the Hubble constant value of  $73.9 \pm 3.0$  km s<sup>-1</sup> Mpc<sup>-1</sup> reported by the MCP in Pesce et al. (2020a).

<sup>3</sup> A typical megamaser map presents two highly redshifted and blueshifted photon sources situated at the ends the disk midline, and a group of systemic masers coming from the vicinity of the LOS (Lo 2005 and Henkel et al. 2005).

<sup>4</sup> We follow the latter authors and exclude the redshifted data point at the position  $(-0.226, 1.345)$  on the sky from the disk model fitting since it is assumed to be the result of BH outflow or other gas and dust unrelated to the megamaser disk.

For this galaxy we estimated four parameters: the mass-to-distance ratio  $M/D = (1.34 \pm 0.04) \times 10^5 M_{\odot} \text{Mpc}^{-1}$ , which multiplied by the above cited distance  $D = 39.6 \pm 1.6$  Mpc renders a BH mass of  $M = (5.31 \pm 0.27) \times 10^6 M_{\odot}$ , the recession velocity  $v_{rec} = 2887.68^{+7.33}_{-7.29}$  km s<sup>-1</sup>, and the BH position with  $x = 0.09 \pm 0.06$  and  $y = 0.01^{+0.17}_{-0.20}$ , referred to the above mentioned position on the sky. We performed the fitting to obtain these results with a scattering azimuthal angle of 12 degrees, leading to a reduced  $\chi^2 = 1.48$  (see Table 2). We highlight the physically suitable estimated BH position, located just behind the systemic masers (see Fig. 3) as expected.

### 3.3. UGC 3193

The UGC 3193 VLBI map is atypical in the sense that it is localized in four distinct velocity windows and presents a maser disk diameter of 2 – 3 pc, more extended than typical subparsec maser disks (see, Fig. 1). On the other hand, UGC 3193's maser profile displays a remarkable symmetry with respect to the galaxy's recession velocity with no lines detected close to it, evidencing that the maser originates from an edge-on disk in which only highly frequency shifted features are detected. Alternatively, discrete rings or a spiral density pattern in an accretion disk can also reproduce the observed maser map. The lack of maser lines at the systemic velocity suggests that i) the disk inclination or a disk warping prevents beaming of masers into our LOS, or ii) there is no background continuum emission that stimulates the systemic features (see Braatz & Gugliucci 2008). Moreover, the structure of the maser profile shows a pronounced kink formed by the highly redshifted and blueshifted maser spots. The distance to this galaxy  $D = 60.3 \pm 2.5$  Mpc was computed using the HI line velocity of  $4454 \pm 10$  km s<sup>-1</sup> and the the MCP's Hubble constant value of  $73.9 \pm 3.0$  km s<sup>-1</sup> Mpc<sup>-1</sup> (see Pesce et al. 2020a).

For this galaxy we estimated three parameters: the mass-to-distance ratio  $M/D = (0.18 \pm 0.01) \times 10^5 M_{\odot} \text{Mpc}^{-1}$  that yields a BH mass of  $M = (1.09 \pm 0.08) \times 10^6 M_{\odot}$  upon multiplication by the above mentioned distance  $D = 60.3 \pm 2.5$  Mpc, the recession velocity  $v_{rec} = 4429.31^{+1.93}_{-1.91}$  km s<sup>-1</sup>, and the  $x$ -offset of the BH position on the sky  $x = 0.05 \pm 0.06$  with respect to the above mentioned reference point. We performed the fitting of these parameters with a scattering azimuthal angle of 22 degrees, leading to a reduced  $\chi^2 = 1.56$  (see Table 2). The resulting  $x$ -offset of the BH position is physically meaningful in the sense that it is located at a central position with respect to the highly redshifted and blueshifted maser features (see Fig. 4).

### 3.4. Gravitational redshifts

It is worth mentioning that one of the virtues of the general relativistic method used to estimate the parameters of BHs hosted in the core of AGNs is that it allows for the clear identification of the relativistic effects present in their dynamics. In particular, it enables the gravitational redshift of each highly redshifted or blueshifted maser feature to be quantified. This fact eases the potential detection of such a general relativistic effect in this kind of astrophysical systems. Therefore, as an application of this formalism, we calculate the gravitational redshift of the closest masers to the BHs located at the center of the IC 2560 and UGC 3193 galaxies and display the corresponding results in Table 3.

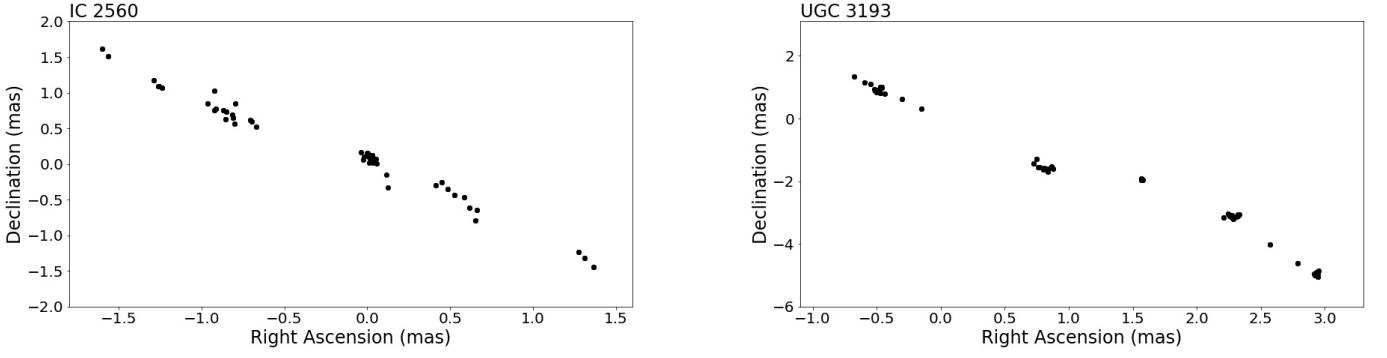


**Fig. 1.** Position maser distribution for IC 2560 and UGC 3193 galaxies.

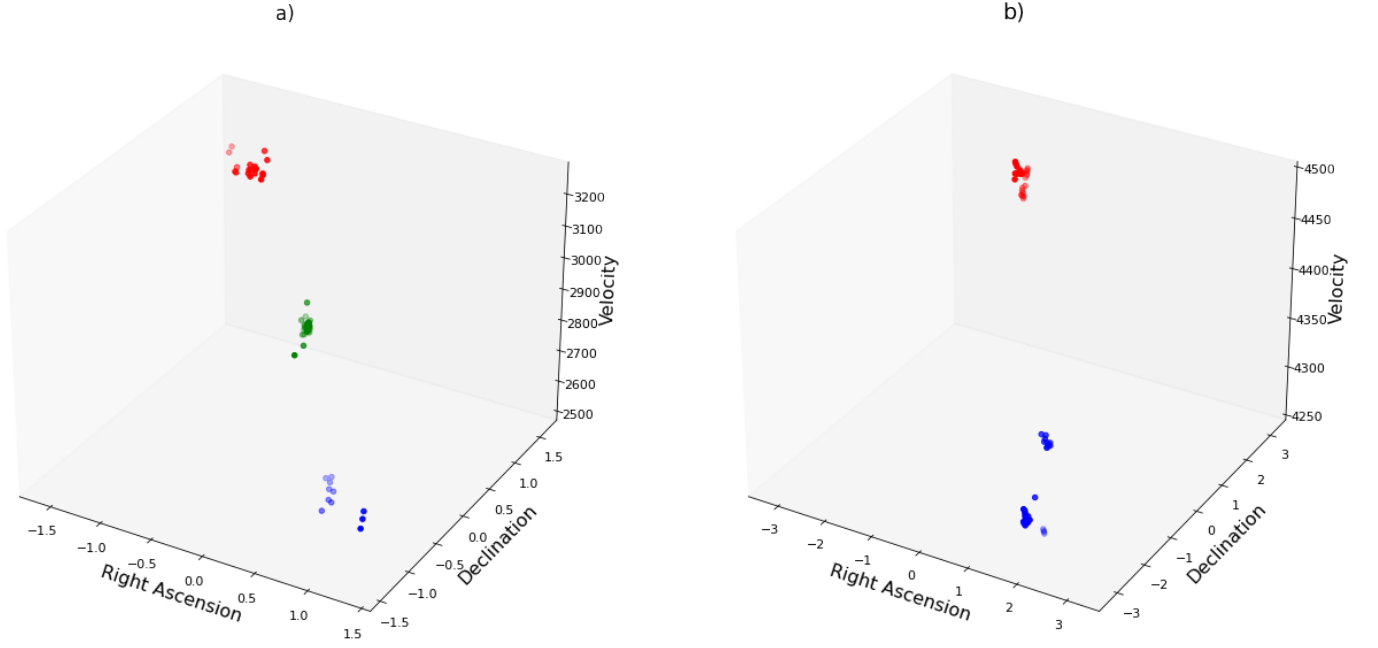


**Fig. 2.** Velocity-Position maser distribution for a) IC 2560 and b) UGC 3193 galaxies.

**Table 1.** Previously reported parameters of the BH living in IC 2560 and UGC 3193 AGNs.

Source	Position R.A. ( $^h : ^m : ^s$ ) Decl. ( $^\circ : ' : ''$ )	Mass ( $10^6 M_\odot$ )	Distance (Mpc)	$M/D$ ( $10^5 M_\odot$ )/Mpc	Recession velocity (km/s)
IC 2560	10:16:18.710 -33:33:49.74	$5.3 \pm 0.2^*$	$39.3^{+1.2}_{-0.9}^*$	1.35	$2923 \pm 10$
UGC 3193	04:52:52.6 +03:03:26	$1.20 \pm 0.03^\dagger$	$60.3 \pm 2.5$	0.20	$4454 \pm 10$

**Notes.** Column 1: Name of the source. Column 2: Source position (J2000). Column 3: Mass of the supermassive BH. Column 4: Distance to the source. Column 5: Computed  $M/D$  ratio from Columns 3 and 4. Column 6: Recession velocity of the galaxies as a whole entity.

Label \* indicates quantities estimated by Kaliszewski & Braatz (2021) with the dataset reported in their work.

Label  $^\dagger$  denotes an upper limit on the BH mass set by Kaliszewski & Braatz (2021).

#### 4. Concluding remarks

In this work, we employed a general relativistic method to estimate the  $M/D$  ratio of the central BH hosted at the core of the IC 2560 and UGC 3193 galaxies, along with their recession velocity and position on the sky. The  $M/D$  ratio of the central BH

of IC 2560 is  $M/D = (1.34 \pm 0.04) \times 10^5 M_\odot \text{Mpc}^{-1}$ , whereas the one of UGC 3193 reads  $M/D = (1.8 \pm 0.1) \times 10^4 M_\odot \text{Mpc}^{-1}$ . We further used the distances indicated in Table 2 and propagated the corresponding uncertainties for each galaxy to compute the BH mass  $M = (5.31 \pm 0.27) \times 10^6 M_\odot$  for IC 2560

**Table 2.** Best fitted parameter values of our estimations.

Source	$M/D$ ( $10^5 M_\odot/\text{Mpc}$ )	$D^a$ (Mpc)	$M$ ( $10^6 M_\odot$ )	$x_0$ (mas)	$y_0$ (mas)	$z_{rec}$ ( $10^{-3}$ )	$v_{rec}$ (km/s)	$\varphi$ ( $^\circ$ )	$\chi^2_{red}$
IC 2560	$1.34 \pm 0.04$	$39.6 \pm 1.6$	$5.31 \pm 0.27$	$0.09 \pm 0.06$	$0.01^{+0.17}_{-0.20}$	$9.63 \pm 0.02$	$2887.68^{+7.33}_{-7.29}$	12	1.48
UGC 3193	$0.18 \pm 0.01$	$60.3 \pm 2.5$	$1.09 \pm 0.08$	$0.05 \pm 0.06$	$-0.06^b$	$14.77 \pm 0.01$	$4429.31^{+1.93}_{-1.91}$	22	1.56

**Notes.** Column 1: Name of the source. Column 2: Fitted mass-to-distance ratio. Column 3: Distance to the galaxy. Column 4: Computed mass from values in Columns 2 and 3. Column 5: Horizontal offset ( $x_0$ ) of the BH position yielded by the Bayesian fit. Column 6: Vertical offset ( $y_0$ ) of the BH position either rendered by the Bayesian fit or fixed. Column 7: Recessional redshift obtained by the fit. Column 8: Recession velocity associated to the recessional redshift after the optical definition. Column 9: Scattering in the azimuthal angle. Column 10: Reduced  $\chi^2$  of the best fit.

Label <sup>a</sup> indicates that the distances were calculated in Kaliszewski & Braatz (2021).

Label <sup>b</sup> indicates that we fixed the vertical offset ( $y_0$ ) of the BH position with the centroid of the complete maser dataset.

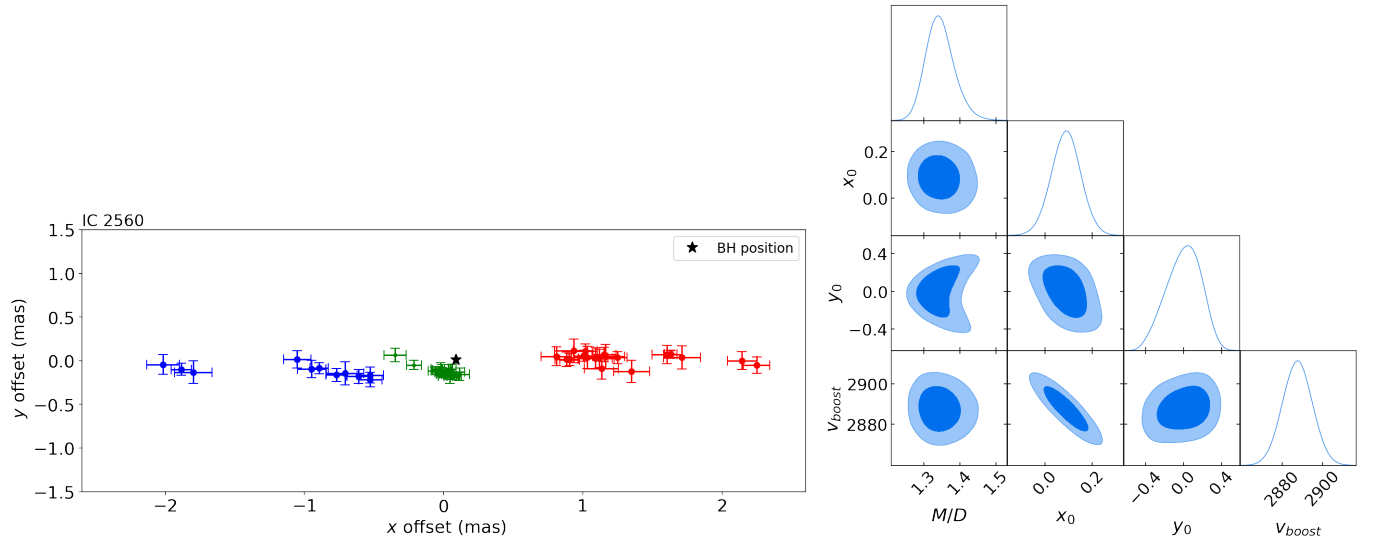


**Fig. 3.** Edge-on view of the maser map and posterior probability distribution of the IC 2560 AGN. The maser disk displays three groups of features with their corresponding observational errors. The star symbol indicates the best fit value for the BH position on the sky with its uncertainties. The blue graphs in the right panel shows the posterior probability distribution with contour levels corresponding to  $1\sigma$  and  $2\sigma$  confidence regions.

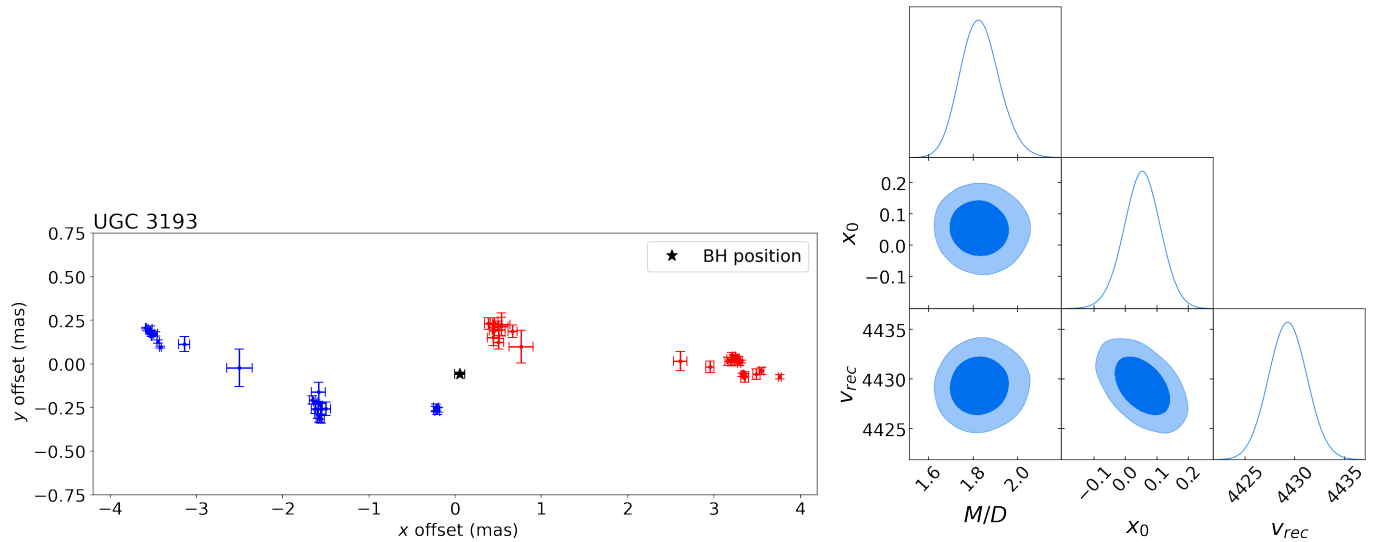


**Fig. 4.** Maser map and posterior probability distribution for the galaxy UGC 3193. The maser map shows the edge-on view of two groups of maser features with their corresponding errors. The black star symbol stands for the best fit value of the  $x$ -offset of the BH position on the sky along with its uncertainty. The right panel displays the posterior probability distribution with contour levels corresponding to  $1\sigma$  and  $2\sigma$  confidence regions.

**Table 3.** Gravitational redshift of the closest masers to the BHs.

Source	Maser feature	Distance to closest maser (mas)	Gravitational redshift ( $10^{-6}$ )	Associated velocity (km/s)
IC 2560	Blue	0.64	3.10	0.93
UGC 3193	Blue	0.32	0.84	0.25

and  $M = (1.09 \pm 0.08) \times 10^6 M_{\odot}$  for UGC 3193. The latter value constitutes the first BH mass reported in the literature for the UGC 3193 AGN. These masses correspond to supermassive BHs. Thus, the megamaser systems that host these BHs are typical in the sense that their masses lie within the range  $10^6 - 10^7 M_{\odot}$ .

In principle, we found that our best fitted values are in accordance with the estimated mass for the BH living in IC 2560 and the BH mass upper limit of UGC 3193 reported by Kaliszewski & Braatz (2021). Namely, our calculated value for the BH mass of IC 2560 practically coincides with the one obtained by these authors for the fit performed taking into account all the maser components of the system  $M = (5.3 \pm 0.2) \times 10^6 M_{\odot}$ ; on the other hand, for the UGC 3193 AGN our computed value approaches the upper limit of the BH mass  $M = (1.20 \pm 0.03) \times 10^6 M_{\odot}$  obtained for the fit trial that considers both the inner and outer components of the maser system in their classification.

In relation to the recession velocities we observe that for the IC 2560 galaxy our best fit value  $v_{rec} = 2887.68^{+7.33}_{-7.29}$  km s $^{-1}$  is less than the 21 cm line velocity of the galaxy  $2923 \pm 10$  km s $^{-1}$ , in magnitude and slightly in error. For the UGC 3193 galaxy we obtained a best estimated value  $v_{rec} = 4429.31^{+1.93}_{-1.91}$  km s $^{-1}$  lower than the HI line velocity of the galaxy  $4454 \pm 10$  km s $^{-1}$ , both in magnitude and error. The difference between these velocities amounts to  $\sim 25$  km s $^{-1}$  and we would like to highlight that the error of our best fit value is considerable less than the error of the galaxy's HI line velocity.

Additionally, we computed the gravitational redshift of the closest maser to the BH for both galaxies according to our best fit BH position values. The results are displayed in Table 3 and account for an order of magnitude weaker gravitational redshifts when compared to those of most of the BHs hosted at the nucleus of the AGNs previously studied by the MCP and reported in Villaraos et al. (2022) and González-Juárez et al. (2024) as well as to that of the NGC 4258 galaxy analyzed in Nucamendi et al. (2021).

*Acknowledgements.* The authors are grateful to D. Villaraos, U. Nucamendi and M. Momennia for illuminating discussions. The authors thank A. Kaliszewski and J. Braatz for making the observational data used in this work publicly available and acknowledge CONAHCYT for support under grant No. CF-MG-2558591 as well as SNIH. A.G.-J. was supported by a postdoctoral grant under the CONAHCYT program *Estancias Posdoctorales por México 2022*, whereas A.H.-A. acknowledges support from VIEP-BUAP.

## References

Kormendy, J., Richstone, D., 1995, *Annu. Rev. Astron. Astrophys.*, 33, 581  
 Celotti, A., Miller, J. C., Sciamia, D. W., 1999, *Class. Quantum Grav.*, 16, A3  
 Kormendy, J., Ho L. C., 2013, *Ann. Rev. Astron. Astrophys.*, 51, 511

Greene, J. E., Seth, A., Kim, M., Läscher, R., Goulding, A., Gao, F., Braatz, J. A., Henkel, C., Condon, J., Lo, K. Y., Zhao, W., 2016, *ApJL*, 826, L32  
 Wardle M., Yusef-Zadeh F., 2012, *ApJL*, 750, L38  
 Gao, F., Braatz, J. A., Reid, M. J., Lo, K. Y., Condon, J. J., Henkel, C., Kuo, C. Y., Impellizzeri, C. M. V., Pesce, D. W., Zhao, W., 2016, *ApJ*, 817, 128  
 Gao, F., Braatz, J. A., Reid, M. J., Condon, J. J., Greene, J. E., Henkel, C., Impellizzeri, C. M. V., Lo, K. Y., Kuo, C. Y., Pesce, D. W., Wagner, J., Zhao, W., 2016, *ApJ*, 834, 52  
 C. Y. Kuo, F. Gao, J. A. Braatz, D. W. Pesce, E. M. L. Humphreys, M. J. Reid, C. M. V. Impellizzeri, C. Henkel, J. Wagner, C. E. Wu, What Determines the Boundaries of H<sub>2</sub>O Maser Emission in an X-ray Illuminated Gas Disk?, 2023, arxiv: 2312.16382 [astro-ph.GA]  
 Reid, M.J., Braatz, J.A., Condon, J.J., Greenhill, L.J., Henkel, C., Lo, K.Y., 2009, *ApJ*, 695, 287  
 Kuo, C. Y., Braatz, J. A., Condon, J. J., Impellizzeri, C. M. V., Lo, K. Y., Zaw, I., Schenker, M., Henkel, C., Reid, M. J., Greene, J. E., 2011, *ApJ*, 727, 20  
 Kuo, C. Y., Braatz, J. A., Reid, M. J., Lo, K. Y., Condon, J. J., Impellizzeri, C. M. V., Henkel, C., 2013, *ApJ*, 767, 155  
 Zhao, W., Braatz, J. A., Condon, J. J., Lo, K. Y., Henkel, C., Pesce, D. W., Greene, J. E., Gao, F., Kuo, C. Y., Impellizzeri, C. M. V., 2018, *ApJ*, 854, 124  
 Pesce, D. W., Braatz, J. A., Reid, M. J., Condon, J. J., Gao, F., Henkel, C., Kuo, C. Y., Lo, K. Y., and Zhao, W., 2020, *ApJ*, 890, 118  
 Kuo, C. Y., Braatz, J. A., Impellizzeri, C. M. V., Gao, F., Pesce, D., Reid, M. J., Condon, J., Kamali, F., Henkel, C., Greene, J. E., 2020, *MNRAS*, 498, 1609  
 Pesce, D. W., Braatz, J. A., Reid, M. J., Riess, A. G., Scolnic, D., Condon, J. J., Gao, F., Henkel, C., Impellizzeri, C. M. V., Kuo, C. Y., and Lo, K. Y., 2020, *ApJL*, 891, L1  
 Herrera-Aguilar, A., Nucamendi, U., 2015, *Phys. Rev. D*, 92, 045024  
 Banerjee, P., Herrera-Aguilar, A. Momennia, M., Nucamendi, U., 2022, *Phys. Rev. D*, 105, 124037  
 Nucamendi, U., Herrera-Aguilar, A., Lizardo-Castro, R., López-Cruz, O., 2021, *ApJL*, 917, L14  
 Villalobos-Ramírez, A., Gallardo-Rivera, O., Herrera-Aguilar, A., Nucamendi, U., 2022, *Astron. Astrophys.*, 662, L9  
 Villaraos, D., Herrera-Aguilar, A., Nucamendi, U., González-Juárez, G., Lizardo-Castro, R., 2022, *MNRAS*, 517, 4213  
 González-Juárez, A., Momennia, M., Villalobos-Ramírez, A., and Herrera-Aguilar, A., 2024, *Astron. Astrophys.*, in press.  
 Schutz, B., 2009, *A First Course in General Relativity* (Cambridge University Press, Cambridge) 411  
 Rindler, W., 1982, *Introduction to special relativity* (Clarendon Press, Oxford Science Publications) 192  
 Davis, T. M., Scrimgeour, M. I., 2014, *MNRAS*, 442, 1117  
 Herrnstein, J. R., Moran, J. M., Greenhill, L. J., Trotter, Adam S., 2005, *ApJ*, 629, 719  
 Kaliszewski, A., Braatz, J. A., 2021, *Proceedings of the NRAO Summer Student Program*, <https://www.nrao.edu/students/2021/Reports/KaliszewskiAlina.pdf>  
 Lo, K. Y., 2005, *Annu. Rev. Astron. Astrophys.*, 43, 625  
 Henkel, C., Braatz, J. A., Tarchi, A., Peck, A. B., Nagar, N. M., Greenhill, L. J., Wang, M., Hagiwara, Y., 2005, *Ap&SS*, 295, 107  
 Braatz, J. A., Wilson, A. S., Henkel, C., 1994, *AAS Meeting Abstracts*, 26, 1342  
 Nakai, N., Inoue, M., Hagiwara, Y., Miyoshi, M., Diamond, P. J., 1998, in *IAU Colloq. 164, Radio Emission from Galactic and Extragalactic Compact Sources*, ed. J. A. Zensus, G. B. Taylor & J. M. Wrobel (ASP Conf. Ser. 144; San Francisco: ASP), 237  
 Ishihara, Y., Nakai, N., Iyomoto, N., Makishima, K., Diamond, P., Hall, P., 2001, *PASJ*, 53, 215  
 Braatz, J. A., Gugliucci, N. E. 2008, *ApJ*, 678, 96  
 Braatz, J. A., Reid, M. J., Humphreys, E. M. L., Henkel, C., Condon, J. J., Lo, K. Y., 2010, *ApJ*, 718, 657, 2020a  
 Pesce, D., Braatz, J., Reis, M., et al. 2020a, doi:10.5281/zenodo.4062113